Comparative Analysis of MOPSO and MOICA for Multi-Objective Geometric Optimization of Labyrinth Spillways

Nazila Kardan [1]

1. Department of Civil Engineering, Azarbaijan Shahid Madani University, Tabriz, Iran.

***Corresponding Author:**
Nazila Kardan

Email: n.kardan@azaruniv.ac.ir
Received: 2026.05.11
Accepted: 2026.07.27
J. Hydraul. Struct., 13(1):1-27
DOI: 10.22055/jhs.2026.51996.1383

ABSTRACT

Labyrinth spillways are widely used to increase effective crest length and improve discharge capacity where conventional spillway widening is restricted by geometric, structural, or economic limitations. However, identifying an efficient labyrinth configuration remains challenging because hydraulic performance and construction cost are governed by nonlinear interactions among geometric variables. This study develops a scenario-based multi-objective optimization framework for the geometric design of a real-world labyrinth spillway by coupling empirical hydraulic relationships with two evolutionary algorithms: Multi-Objective Particle Swarm Optimization (MOPSO) and Multi-Objective Imperialist Competitive Algorithm (MOICA). The optimization problem was formulated to maximize discharge capacity and minimize concrete volume while satisfying hydraulic, geometric, structural, and design-discharge constraints. Three design scenarios with different levels of geometric freedom were considered to evaluate the influence of constraint severity on the hydraulic response and attainable optimized solutions. The framework was applied to the Ute Dam labyrinth spillway as a benchmark case. Results from ten independent runs showed that MOPSO outperformed MOICA in convergence stability, objective-space coverage, and robustness. MOPSO achieved a higher mean Hypervolume value of 0.721 compared with 0.662 for MOICA, representing an improvement of approximately 8.9%. It also reached Hypervolume stabilization earlier, after 42 iterations compared with 57 iterations for MOICA, and showed a lower Hypervolume standard deviation of 0.009 compared with 0.017. The scenario-based results demonstrated that the most flexible design case produced the most favorable volume–discharge response, whereas excessive geometric enlargement did not necessarily improve hydraulic performance. Increasing concrete volume from 6000 to 9500 m^3 reduced discharge capacity by approximately 3.52–4.41%, and the volume-normalized hydraulic productivity decreased by about 39%. These results indicate that balanced geometric proportions are more important than structural enlargement alone. Overall, the proposed framework provides a reproducible and practical decision-support tool for labyrinth spillway design and rehabilitation, with MOPSO identified as the more reliable primary optimizer and MOICA retained as a complementary benchmark for exploratory solution diversity.

KEYWORDS

Labyrinth spillway; Scenario-based optimization; Multi-objective optimization; Geometric optimization; MOPSO; MOICA; Hypervolume indicator; Discharge capacity; Concrete volume; Hydraulic productivity; Ute Dam.

1 Introduction

Spillways are among the most critical hydraulic structures in dam and reservoir systems because they provide a controlled passage for excess floodwater and directly affect dam safety, reservoir operation, and downstream flood-risk management. In recent decades, aging dam infrastructure, revised flood estimates, climate-related hydrological uncertainty, and stricter safety requirements have increased the need for cost-effective spillway upgrading and rehabilitation. However, increasing the capacity of conventional linear spillways by widening the crest is often restricted by site topography, structural limitations, reservoir-operation constraints, environmental considerations, and construction cost [1–3].

Labyrinth spillways provide an effective alternative when additional discharge capacity is required within a limited channel width. By folding the crest in plan view, these structures increase the developed crest length and can pass larger discharges under a given upstream head compared with a conventional straight weir of the same available width. The hydraulic advantage of labyrinth spillways has been widely documented in experimental, analytical, and design-oriented studies [4–6]. More recently, comprehensive reviews have emphasized the continued importance of labyrinth and piano-key weirs for spillway rehabilitation, capacity improvement, and future hydraulic-structure design [9, 25].

Despite their hydraulic advantages, the performance of labyrinth spillways is strongly dependent on geometric proportions. Key parameters include the number of cycles, developed crest length, sidewall angle, apex width, cycle width, weir height, wall thickness, crest shape, and relative head ratio. Previous studies have shown that labyrinth spillways are generally more efficient at relatively low head ratios, whereas their efficiency may decrease at higher heads because of nappe interference, local submergence, flow contraction, and reduced effective crest-length contribution [4, 5, 24, 25]. Therefore, increasing the structural dimensions or the total concrete volume does not necessarily result in improved hydraulic performance unless the geometric proportions remain hydraulically efficient.

The hydraulic behavior of labyrinth spillways is highly nonlinear because the discharge coefficient is affected by complex interactions among head ratio, crest length, cycle geometry, approach flow, and local flow separation. Empirical and semi-empirical formulations remain useful for preliminary design and optimization because they provide computationally efficient estimates of discharge capacity. However, recent numerical studies have shown that three-dimensional flow features such as nappe interaction, recirculation zones, flow separation near apexes, and free-surface deformation can significantly influence the hydraulic efficiency of nonlinear weirs. CFD-based studies have therefore provided valuable insight into the hydraulic performance of labyrinth and piano-key spillway systems under different geometric and flow conditions [7–9, 26].

In addition to experimental and CFD-based studies, optimization techniques have increasingly been used to improve the design of labyrinth spillways and related hydraulic structures. Earlier optimization studies mainly focused on single-objective formulations, such as minimizing concrete volume or maximizing discharge capacity, using methods such as Genetic Algorithms, Particle Swarm Optimization, Bat Algorithm, Whale Optimization Algorithm, and other metaheuristic approaches [10–13]. Reliability-based and hybrid optimization approaches have also been applied to labyrinth spillway design, indicating the growing role of uncertainty-aware and advanced metaheuristic methods in hydraulic-structure optimization [13]. Although these studies have provided valuable design improvements, single-objective optimization cannot fully represent the conflicting nature of hydraulic and economic objectives in practical

spillway design.

More recent research has moved toward multi-objective and data-driven formulations. For example, multi-objective optimization combined with artificial neural networks has been used to improve labyrinth spillway design while predicting the discharge coefficient [14]. Related studies have also shown that machine-learning and hybrid prediction models can improve the estimation of discharge coefficients for nonlinear weirs and support more efficient design exploration [28]. Furthermore, recent experimental investigations on trapezoidal labyrinth weirs have emphasized that geometric configuration affects not only hydraulic efficiency but also downstream scour behavior, confirming the importance of integrated geometric assessment in practical design [27].

The practical design of labyrinth spillways requires balancing at least two conflicting objectives: maximizing discharge capacity and minimizing construction cost. Designs with larger geometric dimensions may increase concrete volume and construction cost, while overly compact designs may fail to provide the required hydraulic capacity. Multi-objective optimization is therefore more suitable than single-objective optimization because it produces a set of non-dominated Pareto-optimal solutions rather than a single design. This enables engineers to evaluate trade-offs between hydraulic performance and construction economy and to select a compromise solution based on project-specific priorities. Quantitative indicators such as Spacing, Generational Distance, and Hypervolume can further support objective comparison of optimization algorithms in terms of convergence, diversity, distribution uniformity, and robustness [20–22].

Although considerable progress has been made, several research gaps remain. First, direct comparative studies between different multi-objective evolutionary algorithms for labyrinth spillway geometry are still limited, particularly for Multi-Objective Particle Swarm Optimization (MOPSO) and Multi-Objective Imperialist Competitive Algorithm (MOICA). Second, many previous studies have considered idealized or laboratory-scale geometries, whereas fewer studies have examined real-world spillway configurations with practical geometric and structural constraints. Third, the effect of design freedom on Pareto-front quality has not been sufficiently investigated through scenario-based optimization. Fourth, counter-intuitive outcomes, such as reduced discharge capacity despite increased concrete volume, require further interpretation because they may be associated with unfavorable geometric proportions, reduced discharge coefficient, nappe interference, or limitations of empirical hydraulic formulations [5, 24, 25].

To address these gaps, the present study develops a scenario-based multi-objective optimization framework for the geometric design of labyrinth spillways. The framework integrates established empirical hydraulic relationships with two population-based evolutionary algorithms, namely MOPSO and MOICA. The optimization problem is formulated to maximize discharge capacity while minimizing concrete volume under hydraulic, geometric, and structural constraints. Three design scenarios with different levels of geometric freedom are considered to evaluate how constraint severity affects the attainable Pareto-optimal solutions and the final engineering trade-offs.

The Ute Dam labyrinth spillway is adopted as a real-world benchmark case because of its documented prototype geometry, rehabilitation background, and relevance to high-capacity spillway design. Unlike studies that focus only on a single optimal geometry, the present study evaluates the full Pareto front and compares algorithmic performance using convergence behavior, Hypervolume, solution stability, and scenario-based design interpretation. This allows the proposed framework to support both technical comparison of optimization algorithms and practical

decision-making in hydraulic engineering design.

The main contributions of this study are as follows: (i) development of a reproducible multi-objective optimization framework for labyrinth spillway geometry using empirical hydraulic relationships and explicit design constraints; (ii) direct comparison of MOPSO and MOICA for a constrained hydraulic-structure optimization problem; (iii) scenario-based evaluation of the influence of geometric design freedom on Pareto-front quality and design trade-offs; (iv) quantitative assessment of algorithmic performance using Hypervolume, convergence behavior, and robustness across independent runs; and (v) engineering interpretation of optimized solutions for the Ute Dam labyrinth spillway as a real-world case study.

2 Materials and Methods

2.1 Governing Hydraulic Relationships of Labyrinth Spillways

The hydraulic performance of the labyrinth spillway was evaluated using the standard free-overflow weir discharge equation modified by the developed crest length of the labyrinth planform:

$$Q = \frac{2}{3} C_d L_c \sqrt{2g} H_T^{\frac{2}{3}} \quad (1)$$

where Q is the discharge (m^3/s), C_d is the discharge coefficient, L_c is the developed or effective crest length of the labyrinth spillway (m), g is the gravitational acceleration (9.81 m/s^2), and H_T is the total upstream head above the spillway crest (m). The term L_c represents the hydraulic advantage of the labyrinth configuration, in which the folded crest increases the effective overflow length within a limited channel width [4-5].

The discharge coefficient C_d accounts for the effects of crest geometry, sidewall angle, cycle configuration, approach flow condition, and relative head. For labyrinth spillways, C_d is not constant and may decrease when the flow is affected by nappe interference, local submergence, or flow contraction. Therefore, the total-head-to-spillway-height ratio (H_T/P) was constrained within the practical operating range of 0.05 and 0.90. P is the spillway height measured from the channel floor to the crest level [5,16-17]. This constraint was imposed to keep all candidate solutions within a hydraulically feasible range. In the proposed optimization framework, Eq. (1) was used to calculate the hydraulic objective function for each feasible geometry generated by the optimization algorithms.

2.2 Design Variables and Geometric Parameters

The hydraulic efficiency of a labyrinth spillway is primarily governed by its geometric configuration. The principal geometric parameters considered in the present study are shown in Figure 1. These parameters define the planform geometry of the spillway and form the basis of the optimization model.

In this study, N denotes the number of labyrinth cycles. Increasing N generally increases the developed crest length and may improve discharge capacity; however, an excessive number of cycles may also intensify nappe interference, increase construction complexity, and reduce hydraulic efficiency. The parameter B represents the cycle length, defined as the longitudinal projection of one labyrinth cycle in the flow direction. For consistency, the notation used in the optimization model is defined as follows: A is the apex width, B is the cycle length, w is the cycle width, W_T is the total spillway or channel width, P is the spillway height, t_w is the wall thickness, N is the number of cycles, $\propto$ is the sidewall angle, and L_c is the total effective crest length.

The spillway height is denoted by P, measured vertically from the spillway floor to the crest elevation. This parameter directly affects the relative head ratio H_T/P and therefore plays an important role in the hydraulic performance of the spillway. The wall thickness is denoted by t_w, which

mainly affects structural stability, constructability, and concrete volume. The sidewall angle ∝ is also considered as a key geometric parameter because it controls the orientation of the labyrinth sidewalls and influences both the developed crest length and the flow pattern over the spillway.

The effective crest length L_c represents the total developed length of the folded crest. This parameter is the main source of the hydraulic advantage of labyrinth spillways compared with conventional linear weirs. Nevertheless, increasing L_c does not necessarily lead to a proportional increase in discharge capacity, because unfavorable geometric proportions may reduce the discharge coefficient through nappe interference, local flow contraction, or submergence effects.

For consistency, the notation used in the optimization model is defined as follows: A is the apex width and W_T is the total spillway/channel width, B is the cycle length, w is the cycle width, P is the spillway height, t_w is the wall thickness, N is the number of cycles, ∝ is the sidewall angle, and L_c is the effective crest length. In the proposed framework, these geometric parameters were either treated as design variables or fixed according to the selected optimization scenario. The optimization process aimed to determine the most favorable combination of geometric parameters that maximizes discharge capacity while satisfying all imposed hydraulic, geometric, and structural constraints.

2.3 Formulation of the Multi-Objective Optimization Problem

In this study, the geometric design of the labyrinth spillway was formulated as a constrained multi-objective optimization problem. The two conflicting objectives were to maximize the discharge capacity and minimize the concrete volume. Therefore, the optimization framework aimed to generate a set of non-dominated Pareto-optimal solutions that represent the trade-off between hydraulic performance and construction economy.

The multi-objective optimization problem can be expressed as:

$$\mathrm{F(x)} = [f_1(X), f_2(X)] \quad (2)$$

subject to

$$\mathrm{g}_i(X) \leq 0, \qquad i = 1,2,\dots,m \quad (3)$$

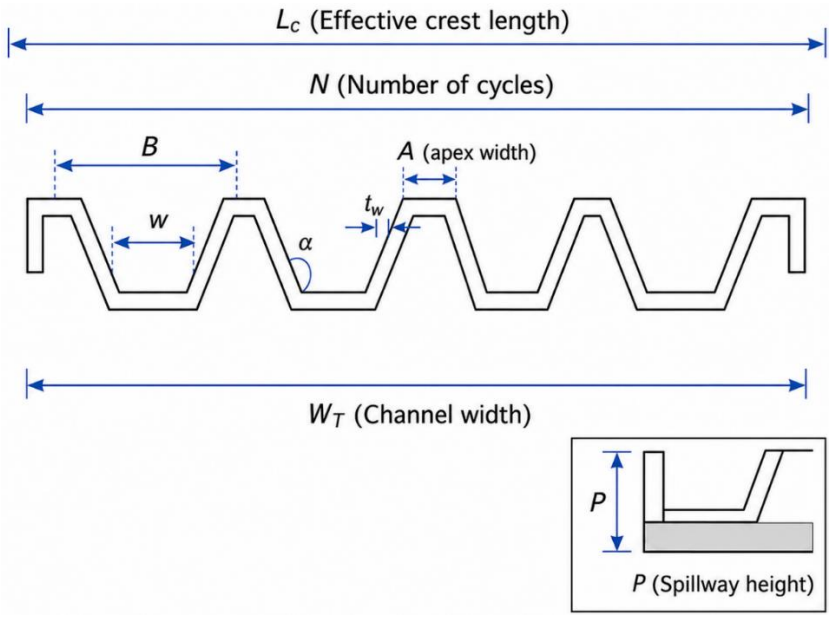


Figure 1. Schematic representation of the labyrinth spillway geometry showing the principal design variables and geometric parameters used in the optimization model.

where F(x) is the vector of decision variables, $f_1(X)$ and $f_2(X)$ are the objective functions, and $g_i(X)$ represents the i^{th} normalized design constraint.
The decision vector was defined as:

$$X = [\alpha \; B \; A \; P \; t_w \;\; N] \quad (4)$$

where α is the sidewall angle, B is the cycle length, A is the apex width, P is the spillway height, t_w is the wall thickness, and N is the number of labyrinth cycles. The sidewall angle was defined in degrees in the design-variable bounds, but it was converted to radians when evaluating trigonometric functions in the optimization model.
The cycle width was calculated as:

$$\omega = 2(B\tan\alpha + A) \quad (5)$$

The total spillway width was obtained as:

$$W_T = N\omega = 2N(B\tan\alpha + A) \quad (6)$$

The crest length per cycle was calculated as:

$$l_c = 2\left(\frac{B}{\cos\alpha} + A\right) \quad (7)$$

Accordingly, the total developed or effective crest length was expressed as:

$$L_c = Nl_c = 2N\left(\frac{B}{\cos\alpha} + A\right) \quad (8)$$

The first objective function was defined to maximize the discharge capacity. Based on the free-overflow equation, the discharge capacity of each candidate geometry was calculated as:

$$Q(X) = \frac{2}{3}C_d L_c\sqrt{2g}H_T^{3/2} \quad (9)$$

By substituting Eq. (9) into Eq. (10), the discharge capacity can be written as:

$$Q(X) = \frac{2}{3}C_d\sqrt{2g}H_T^{3/2}\left[2N\left(\frac{B}{\cos\alpha} + A\right)\right] \quad (10)$$

where Q is the discharge capacity (m^3/s), C_d is the discharge coefficient, g is the gravitational acceleration ($9.81 \sim m/s^2$), and H_T is the total upstream head above the spillway crest. Therefore, the hydraulic objective function was expressed as:

$$f_1(X) = \max Q(X) \quad (11)$$

For implementation in a minimization-based optimization framework, the same objective can equivalently be written as:

$$f_1(X) = -Q(X) \quad (12)$$

The second objective function was defined to minimize the total concrete volume. Assuming that the dominant concrete volume is associated with the developed wall length, spillway height, and wall thickness, the concrete volume was calculated as:

$$V_c(X) = L_c P t_w \quad (13)$$

or equivalently:

$$V_c(X) = 2N\left(\frac{B}{\cos\alpha} + A\right)Pt_w \quad (14)$$

Thus, the economic objective function was defined as:

$$f_2(X) = \min V_c(X) \quad (15)$$

The allowable ranges of the decision variables used in the optimization model are summarized in Table 1.

Table 1. Design variables and their allowable ranges used in the optimization model.

Variable	Description	Lower bound	Upper bound
α	Sidewall angle (degree)	6°	35°
B	Cycle length (m)	1.0	6.0
A	Apex width (m)	0.1	1.0
P	Spillway height (m)	1.0	5.0
t^w	Wall thickness (m)	0.2	1.0
N	Number of cycles	2	12

To ensure hydraulic feasibility, geometric consistency, structural practicality, and compliance with the required design discharge, a set of normalized constraints was imposed on the optimization model. A candidate solution was considered feasible only when all constraints satisfied:

$$g_i(X) \leq 0 \quad (16)$$

The hydraulic head ratio was constrained as:

$$0.05 \leq \frac{H_T}{P} \leq 0.90 \quad (17)$$

This constraint was implemented through the following normalized forms:

$$g_1(X) = \frac{H_T}{P} \times \frac{1}{0.9} - 1 \leq 0 \quad (18)$$

$$g_2(X) = 1 - \frac{H_T}{P} \times \frac{1}{0.05} \leq 0 \quad (19)$$

The cycle-width-to-height ratio was constrained as:

$$2 \leq \frac{\omega}{P} \leq 4 \quad (20)$$

where (w) is calculated from Eq. (6). The corresponding normalized constraints were:

$$g_3(X) = \frac{\omega}{P} \times \frac{1}{4} - 1 \leq 0 \quad (21)$$

$$g_4 = 1 - \frac{\omega}{P} \times \frac{1}{2} \leq 0 \quad (22)$$

The apex-width ratio was constrained as:

$$\frac{A}{P\omega} \leq 0.08 \quad (23)$$

$$g_5(X) = \frac{A}{\omega} \times \frac{1}{0.08} - 1 \leq 0 \quad (24)$$

The magnification ratio was defined as the ratio of the total developed crest length to the total spillway width:

$$M = \frac{L_c}{W_T} = \frac{l_c}{\omega} \quad (25)$$

where $(W_T = N\omega)$. This ratio was constrained as:

$$3.0 \leq M \leq 9.5 \quad (26)$$

The corresponding normalized constraints were:

$$g_6(X) = \frac{M}{1} \times \frac{1}{9.5} - 1 \leq 0 \quad (27)$$

$$g_7(X) = 1 - \frac{M}{1} \times \frac{1}{3} \leq 0 \quad (28)$$

The structural wall constraint was defined as:

$$1.0 \leq \frac{A}{t_w} \leq 2.0 \quad (29)$$

and was imposed using:

$$g_8(X) = \frac{A}{t_w} \times \frac{1}{2} - 1 \leq 0 \quad (30)$$

$$g_9(X) = 1 - \frac{A}{t_w} \times \frac{1}{1} \leq 0 \quad (31)$$

Finally, the design discharge constraint was imposed to ensure that the optimized spillway satisfies the required design discharge Q_d:

$$Q(X) \geq Q_d \quad (32)$$

which was implemented as:

$$g_{10}(X) = 1 - \frac{Q(X)}{Q_d} \leq 0 \quad (33)$$

or, by substituting Eq. (11):

$$1 - \frac{\frac{2}{3}\sqrt{2g}C_d H_T^{1.5} N\left(\frac{2B}{cos\alpha} + 2A\right)}{Q_d} \leq 0 \quad (34)$$

All objective functions and constraints were evaluated simultaneously for each candidate solution generated by the MOPSO and MOICA algorithms. Candidate solutions violating one or more constraints were treated using the constraint-handling procedure described in Section 2.5. The resulting feasible non-dominated solutions formed the Pareto front, representing the best trade-offs between discharge capacity and concrete volume.

2.4 Multi-Objective Optimization Algorithms and Implementation Details

Two population-based evolutionary algorithms were implemented to solve the constrained multi-objective optimization problem: Multi-Objective Particle Swarm Optimization (MOPSO) and Multi-Objective Imperialist Competitive Algorithm (MOICA). Both algorithms were selected because they are suitable for nonlinear engineering optimization problems involving multiple conflicting

objectives and bounded design variables. In the present study, each candidate solution represented a complete labyrinth spillway geometry defined by the decision vector $X = [\alpha\ B\ A\ P\ t_w\ \ N]$. For each candidate geometry, the discharge capacity $Q(X)$, concrete volume $V_c(X)$, and all normalized constraints were evaluated.

Because the optimization problem contains two conflicting objectives, the algorithms were designed to approximate a Pareto front rather than a single optimum solution. An external archive $\mathcal{A}$ was used to store feasible non-dominated solutions generated during the search. At each iteration, the archive was updated by merging the previous archive with the newly generated population and retaining only the feasible non-dominated solutions:

$$\mathcal{A}^{t+1} = ND(\mathcal{A}^t \cup \mathcal{P}^{t+1}) \quad (35)$$

Where $\mathcal{A}^t$ is the external archive at iteration t, $\mathcal{P}^{t+1}$ is the population generated at iteration t+1, and ND denotes the feasible non-dominated subset. If the archive size exceeded the predefined maximum capacity, a diversity-preservation procedure was applied to remove solutions located in crowded regions of the objective space. In this study, crowding distance was used to preserve the spread and uniformity of the Pareto front:

$$CD_i = \sum_{k=1}^{M} \frac{f_k^{i+1} - f_k^{i-1}}{f_k^{max} - f_k^{min}} \quad (36)$$

Where CD_i is the crowding distance of the i[th] archive member, M is the number of objective functions, f_k^{i+1} and f_k^{i-1} are the neighboring objective values after sorting the archive according to the k[th] objective, and f_k^{max} and f_k^{min} are the maximum and minimum values of the k[th] objective in the archive. Archive members with larger crowding distances were preferred because they contributed more to Pareto-front diversity.

2.4.1 Multi-Objective Particle Swarm Optimization

Particle Swarm Optimization was originally introduced by Kennedy and Eberhart [18]. In MOPSO, each particle represents a candidate labyrinth spillway geometry. The position and velocity of the i[th] particle at iteration t are denoted by x_i^t and v_i^t, respectively. Particle movement is guided by its personal best position Pbest_i^t and a leader selected from the external archive.
The velocity of each particle was updated as:

$$v_i^{t+1} = \omega^t v_i^t + c_1 r_1 \left(\text{Pbest}_i^t - x_i^t\right) + c_2 r_2 \left(\text{leader}_i^t - x_i^t\right) \quad (37)$$

$$x_i^{t+1} = x_i^t + v_i^{t+1} \quad (38)$$

where ω^t is the inertia weight at iteration t, c_1 and c_2 are the cognitive and social acceleration coefficients, and r_1 and r_2 are random numbers uniformly distributed in the interval [0,1]. The inertia weight was decreased linearly during the optimization process to improve the balance between exploration and exploitation:

$$\omega^t = \omega_{max} - \left(\frac{\omega_{max} - \omega_{min}}{T_{max}}\right)t \quad (39)$$

where ω_{max} and ω_{min} are the maximum and minimum inertia weights, respectively, and T_{max} is the maximum number of iterations.

The personal best position of each particle was updated based on Pareto dominance and feasibility. If the new position dominated the previous personal best, it replaced it. If neither solution dominated the other, the solution located in a less crowded region of the objective space was preferred. The leader of each particle was selected from the external archive using a diversity-oriented probability:

$$p_i = \frac{CD_i}{\sum_{j=1}^{|\mathcal{A}|} CD_i} \quad (40)$$

where p_i is the selection probability of the i[th] archive member and $|\mathcal{A}|$ is the number of archive members. This strategy increased the probability of selecting leaders from sparsely populated regions of the Pareto front and reduced premature convergence.

After each position update, boundary control was applied to ensure that all design variables remained within their allowable

ranges. The updated particles were then evaluated using the objective functions and constraints defined in Section 2.3. Feasible non-dominated solutions were added to the external archive according to Eq. (34). The MOPSO procedure continued until the maximum number of iterations was reached. The computational procedure of the implemented MOPSO algorithm is shown in Figure 2a.

2.4.2 Multi-Objective Imperialist Competitive Algorithm

The Imperialist Competitive Algorithm was introduced by Atashpaz-Gargari and Lucas [19]. In MOICA, each candidate solution is represented as a country. A set of high-quality countries is selected as imperialists, while the remaining countries are assigned as colonies to form empires. In the present multi-objective implementation, countries were compared using feasibility, Pareto dominance, and diversity contribution.

During the assimilation phase, each colony moved toward its corresponding imperialist according to:

$$x_c^{t+1} = x_c^t + \beta r(x_{imp}^t - x_c^t) \quad (41)$$

where x_c^t is the position of a colony at iteration t, x_{imp}^t is the position of the corresponding imperialist, β is the assimilation coefficient, and r is a random number uniformly distributed in [0,1].

To maintain diversity and reduce the risk of premature convergence, a revolution operator was applied to a predefined fraction of colonies. During revolution, one or more design variables were regenerated within their allowable bounds:

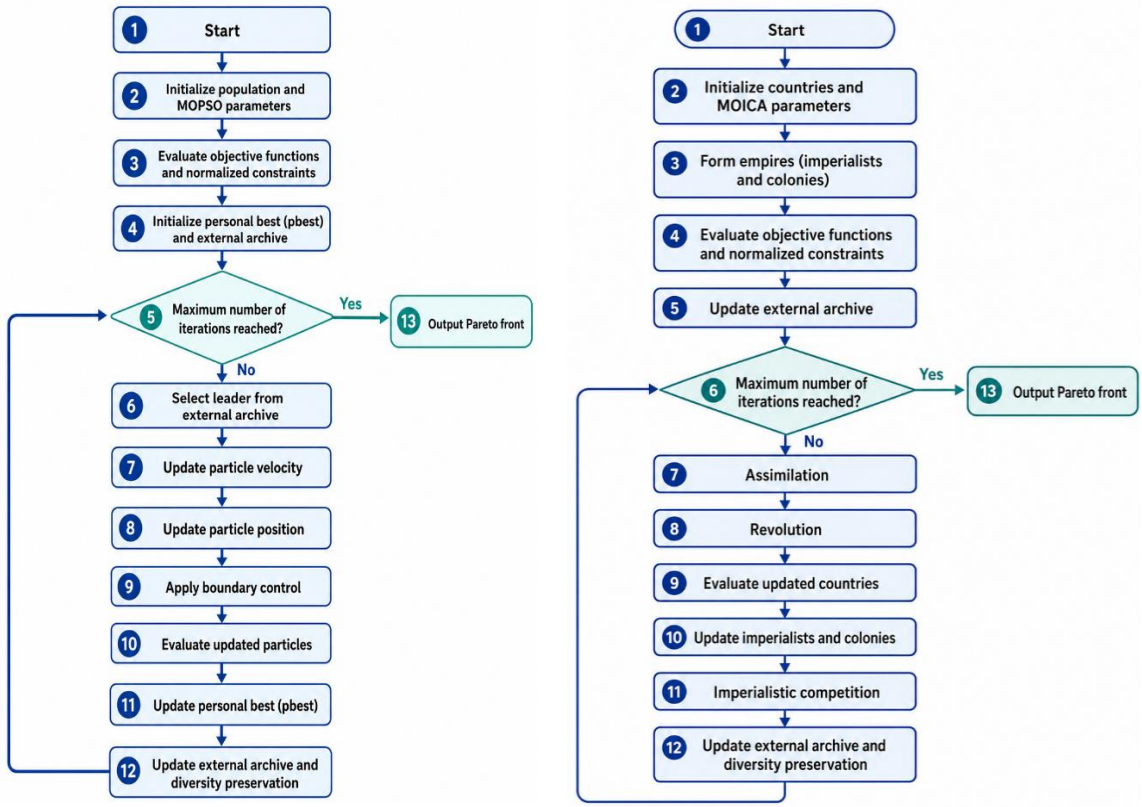
$$x_{i,k}^{t+1} = x_k^L + r(x_k^U - x_k^L) \quad (42)$$

where $x_{i,k}^{t+1}$ is the updated value of the kth design variable of country i, x_k^L and x_k^U are the lower and upper bounds of that variable, and r is a random number uniformly distributed in [0,1].

After assimilation and revolution, all countries were evaluated using the same objective functions and constraints applied in MOPSO. The external archive was updated using Eq. (36), and diversity was preserved using the crowding-distance criterion in Eq. (37). Imperialistic competition was performed by comparing empires based on the quality of their imperialists, the feasibility of their colonies, and their contribution to the non-dominated archive. Weaker empires gradually lost colonies to stronger empires, and collapsed empires were removed from the population. Similar to MOPSO, boundary control was applied after each update to keep all design variables within the feasible search space. The MOICA procedure continued until the maximum number of iterations was reached. The final feasible non-dominated solutions stored in the external archive represented the Pareto-optimal set obtained by MOICA. The computational procedure of the implemented MOICA algorithm is shown in Figure 2b.

2.4.3 Algorithmic Comparison Strategy

To ensure a fair comparison, MOPSO and MOICA were implemented using the same objective functions, design-variable bounds, normalized constraints, population size, archive size, and stopping criterion. Both algorithms were run independently under identical computational conditions. Their performance was compared using convergence behavior, Pareto-front distribution, Hypervolume, and run-to-run stability. This comparison allowed the algorithms to be evaluated not only based on the best solution obtained, but also based on robustness, diversity, repeatability, and practical usefulness for engineering decision-making.



(a) **(b)**

Figure 2. Author-developed computational flowcharts of the optimization algorithms used in the proposed framework: (a) Multi-Objective Particle Swarm Optimization (MOPSO) and (b) Multi-Objective Imperialist Competitive Algorithm (MOICA). The diagrams summarize the main steps for objective and constraint evaluation, archive updating, diversity preservation, iterative solution improvement, and Pareto-front generation.

2.5 Constraint-Handling Strategy

The geometric optimization of labyrinth spillways is a constrained multi-objective problem because each candidate design must satisfy hydraulic, geometric, structural, and design-discharge requirements. Therefore, an explicit constraint-handling strategy was implemented to prevent infeasible configurations from being selected as final Pareto-optimal solutions.

All constraints were first expressed in normalized form as:

$$g_i(X) \leq 0, \quad i = 1,2,\ldots,m \tag{43}$$

where $g_i(X)$ is the normalized value of the i^{th} constraint and m is the total number of constraints. A candidate solution was considered feasible only if all constraints were satisfied. The total constraint violation of a candidate solution was calculated as:

$$CV(X) = \sum_{i=1}^{m} max[0, g_i(X)] \tag{44}$$

where $CV(X)$ is the total constraint violation. Therefore, a feasible solution satisfies:

$$CV(X) = 0 \tag{45}$$

whereas an infeasible solution satisfies:

$$CV(X) > 0 \tag{46}$$

A feasibility-based comparison rule was used during selection, archive updating, personal-best updating, and imperialistic competition. According to this rule, feasible solutions were always preferred over infeasible solutions. When two feasible

solutions were compared, Pareto dominance was used. When two infeasible solutions were compared, the solution with the smaller total constraint violation was preferred. This rule can be summarized as:

$$X_a \prec_c X_b \quad \text{if} \quad \begin{cases} CV(X_a) = 0,\ CV(X_b) > 0 \\ CV(X_a) = 0,\ CV(X_b) = 0,\ X_a \prec_c X_b \\ CV(X_a) < CV(X_b),\ CV(X_b) > 0,\ CV(X_a) > 0 \end{cases} \tag{47}$$

where $\prec_c$ denotes constrained dominance and $\prec$ denotes conventional Pareto dominance.

In addition to constraint violation control, boundary correction was applied after each update of the design variables. If a variable exceeded its allowable lower or upper bound, it was returned to the nearest feasible bound according to:

$$x_{i,k} = \min[\max(x_{i,k}, x_k^L), x_k^U] \tag{48}$$

where $x_{i,k}$ is the value of the kth design variable of candidate solution i, and x_k^L and x_k^U are the corresponding lower and upper bounds. Since the number of cycles N is an integer design variable, its updated value was rounded to the nearest feasible integer after boundary correction:

$$N = round\ (N) \tag{49}$$

subject to:

$$N^L \leq N \leq N^U \tag{50}$$

This constraint-handling procedure ensured that all candidate solutions remained within the physically meaningful and hydraulically feasible design space. It also allowed MOPSO and MOICA to be compared under identical feasibility rules, thereby improving the reproducibility and fairness of the algorithmic comparison.

2.6 Algorithm Parameter Settings and Reproducibility

The performance of population-based metaheuristic algorithms is influenced by the selection of control parameters, including population size, archive size, maximum number of iterations, inertia weight, acceleration coefficients, assimilation coefficient, and revolution rate. To ensure a fair comparison between MOPSO and MOICA, both algorithms were implemented using the same objective functions, design-variable bounds, normalized constraints, archive size, population size, and stopping criterion. The same constraint-handling strategy described in Section 2.5 was also applied to both algorithms.

The population size and maximum number of iterations used in the main optimization analyses were defined as $N_{pop}$and $T_{max} = 200$. Where N_{pop} is the population size and T_{max} is the maximum number of iterations. Therefore, the total number of function evaluations for each independent run was calculated as:

$$N_{FE} = N_{pop} \times T_{max} \tag{51}$$

By substituting the adopted parameter values, the number of function evaluations for each run was $100 \times 200 = 20000$.

The final parameter settings used for the MOPSO and MOICA algorithms are summarized in Table 2. These settings were selected based on common recommendations in the evolutionary optimization literature and preliminary computational checks aimed at achieving stable convergence, adequate Pareto-front coverage, and reasonable computational cost.

Table 2. Parameter settings used for the MOPSO and MOICA algorithms.

Parameter	MOPSO	MOICA
Population size, N_{pop}	100	100
Maximum number of iterations, T_{max}	200	200
Number of function evaluations, N_{FE}	20000	20000
External archive size	100	100
Inertia weight, ω	0.9 to 0.4, linearly decreasing	—
Cognitive coefficient, c_1	2.0	—
Social coefficient, c_2	2.0	—
Number of imperialists	—	10
Assimilation coefficient, β	—	2.0
Revolution rate	—	0.10
Number of independent runs	10	10
Stopping criterion	Maximum iterations	Maximum iterations

To account for the stochastic nature of the algorithms, each algorithm was executed independently over ten runs using the same parameter settings. The final Pareto fronts and performance indicators were then compared in terms of convergence behavior, Hypervolume, solution spread, and run-to-run stability. This procedure ensured that the observed differences between MOPSO and MOICA were attributable to algorithmic behavior rather than inconsistent parameter choices.

The parameter settings reported in Table 2 were kept unchanged for all scenario-based optimization analyses. This consistency was necessary to ensure that differences among scenarios and between algorithms were related to design constraints and search behavior, rather than changes in computational settings. Preliminary trial runs were used only to check the stability of the computational implementation and were not included in the final performance comparison.

2.7 Overall Optimization Framework

The overall optimization framework developed in this study is shown in Figure 3. The framework integrates the hydraulic formulation, geometric relationships, design-variable bounds, normalized constraints, and the two multi-objective optimization algorithms into a unified computational procedure.

The process begins with the definition of the case-study geometry, hydraulic design conditions, and allowable ranges of the decision variables. Each candidate solution is represented by the decision vector $X = [\alpha\ B\ A\ P\ t_w\ \ N]$. Based on this vector, the derived geometric parameters, including cycle width, total spillway width, crest length per cycle, and total effective crest length, are calculated. The discharge capacity $Q(X)$ and concrete volume $V_c(X)$ are then evaluated using the objective functions defined in Section 2.3.

After objective-function evaluation, all hydraulic, geometric, structural, and design-discharge constraints are checked using the normalized constraint functions. Candidate solutions that violate one or more constraints are treated using the feasibility-based constraint-handling strategy described in Section 2.5. Feasible non-dominated solutions are stored in an external archive, and diversity preservation is applied to maintain a well-distributed Pareto front.

Both MOPSO and MOICA follow the same objective functions, constraints, design-variable bounds, population size, archive size, and stopping criterion to ensure a fair comparison. The optimization process continues until the maximum number of iterations is reached. The final output of each algorithm is a set of feasible Pareto-optimal solutions representing the trade-off between maximum discharge capacity and minimum concrete volume.

The resulting Pareto fronts are then

evaluated using convergence behavior, Hypervolume, solution distribution, and robustness across independent runs. This framework enables a systematic comparison between MOPSO and MOICA and provides practical decision-support information for selecting efficient labyrinth spillway geometries under hydraulic and structural constraints.

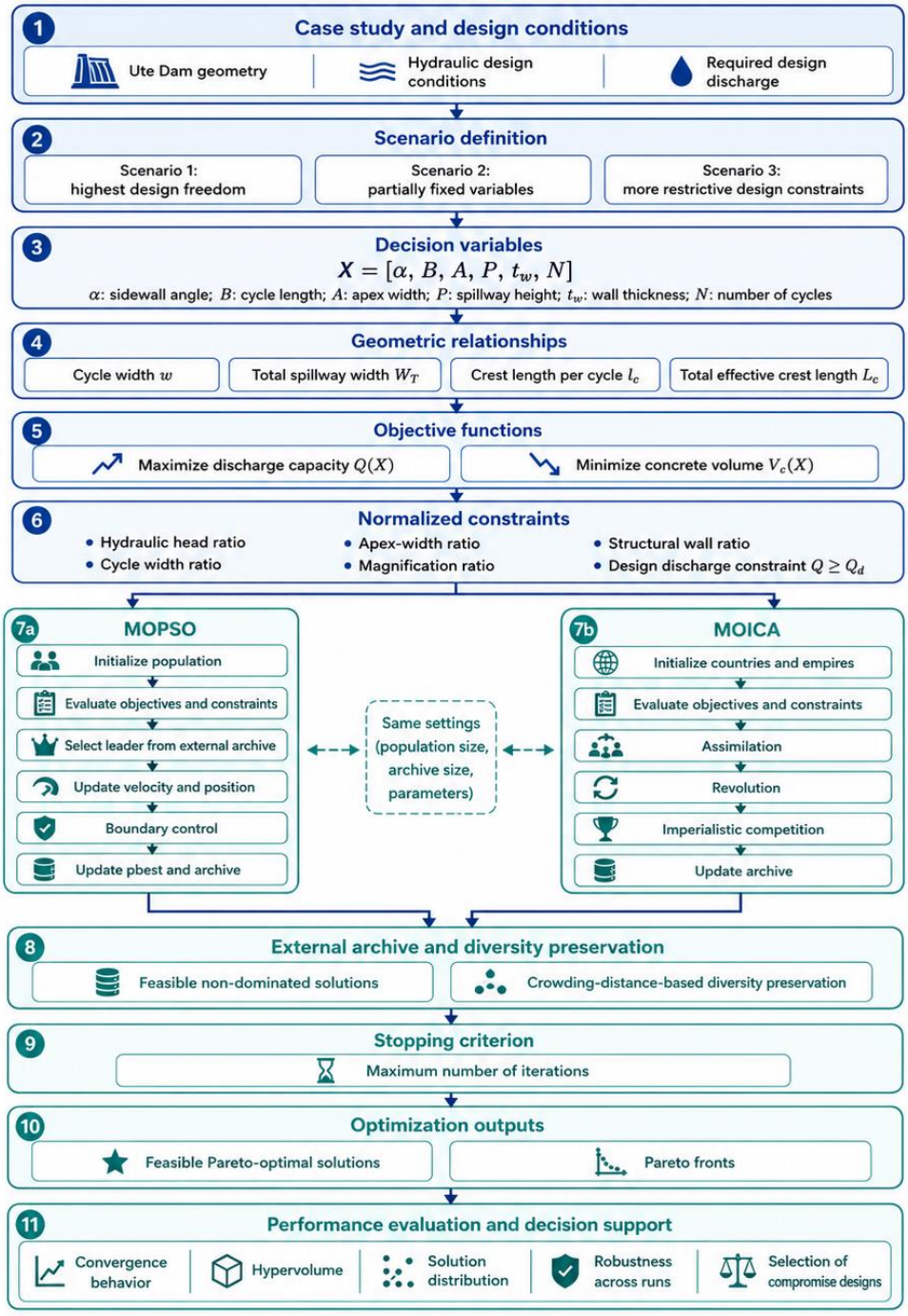


Figure 3. Overall framework of the proposed scenario-based multi-objective optimization procedure for labyrinth spillway design. The framework integrates geometric design variables, hydraulic relationships, objective functions, normalized constraints, MOPSO and MOICA search procedures, external archive updating, Pareto-front generation, and performance evaluation.

3 Case Study, Verification, and Performance Evaluation

3.1 Case Study: Ute Dam Labyrinth Spillway

The Ute Dam labyrinth spillway was selected as the benchmark case study to evaluate the applicability and reliability of the proposed multi-objective optimization framework under real-world hydraulic and geometric conditions. Ute Dam is a zoned earthfill embankment dam constructed on the Canadian River in New Mexico, USA. The spillway rehabilitation project provides a suitable benchmark because its geometry, design constraints, and hydraulic design requirements have been documented and widely used in labyrinth spillway design studies.

The original spillway configuration consisted of an ungated ogee spillway with a limited available channel width. Because conventional capacity improvement by gate installation or major structural expansion was economically and practically constrained, a labyrinth spillway configuration was adopted as a more cost-effective rehabilitation alternative. The final labyrinth layout maintained the available channel width while increasing the developed crest length through a folded planform geometry. This makes the Ute Dam spillway a representative real-world case for assessing the trade-off between hydraulic capacity and structural volume.

The use of Ute Dam as a benchmark is justified for four reasons. First, it represents an actual spillway rehabilitation problem rather than an idealized laboratory configuration. Second, its geometric characteristics provide practical bounds for the optimization variables. Third, the case includes hydraulic and structural constraints that are directly relevant to engineering design. Fourth, it allows the proposed optimization framework to be compared with previously published optimization results based on the same or comparable design conditions.

In the present study, the Ute Dam geometry was used to define the baseline configuration, allowable design-variable ranges, and scenario-specific constraints. The optimization results were interpreted in terms of relative changes in discharge capacity, concrete volume, and Pareto-front quality. Therefore, the calculated discharge values should be understood within the same optimization formulation and design assumptions used for the benchmark comparison, rather than as independent full-prototype hydraulic measurements.

3.2 Optimization Scenarios

To investigate the effect of geometric design freedom on the attainable Pareto-optimal solutions, three optimization scenarios were defined. These scenarios were designed to represent different levels of practical design flexibility, ranging from a relatively flexible rehabilitation design to a more constrained configuration.

In Scenario 1, the number of labyrinth cycles was fixed according to the benchmark spillway configuration, while the remaining geometric variables were optimized within their allowable ranges. This scenario represents the highest level of design freedom considered in the study and was used to examine the maximum achievable improvement under practical geometric constraints.

In Scenario 2, the spillway height and total available spillway width were fixed, while the remaining geometric parameters were optimized. This scenario represents a more realistic rehabilitation condition in which major structural dimensions are constrained by the existing dam geometry and site limitations.

In Scenario 3, the spillway height, total available spillway width, number of cycles, and wall thickness were fixed. Only the remaining geometric parameters were allowed to vary. This scenario represents the most restrictive design case and was used to assess how limited geometric flexibility affects the Pareto front and final compromise solutions.

The three scenarios enabled a systematic

comparison of how constraint severity affects discharge capacity, concrete volume, solution distribution, and the shape of the Pareto front. This scenario-based structure also allowed the optimization framework to provide practical design guidance for both flexible and constrained spillway rehabilitation projects.

3.3 Verification Strategy

The verification procedure was designed to assess whether the proposed computational framework could reproduce previously reported optimization behavior and generate hydraulically feasible labyrinth spillway geometries. The verification was performed in two steps.

First, the baseline formulation was checked by comparing the obtained optimization results with the previously published Genetic Algorithm-based optimization study of Kardan et al. [10]. That study minimized the concrete volume of a labyrinth spillway under hydraulic and geometric constraints and reported a significant reduction in concrete volume relative to the initial design. In the present study, the same baseline design assumptions, hydraulic relationships, and constraint structure were reproduced as closely as possible within the proposed framework. The agreement between the reproduced GA solution and the published reference solution was used as a consistency check for the objective functions, geometric relationships, and constraint implementation.

Second, the verified formulation was solved using MOPSO and MOICA under identical computational settings. Both algorithms used the same objective functions, design-variable bounds, normalized constraints, population size, archive size, maximum number of iterations, and feasibility-based constraint-handling procedure. The parameter settings reported in Table 2 were used for all final optimization comparisons. Preliminary trial runs were used only to check numerical stability and were not included in the final performance evaluation.

The verification comparison was based on the optimized geometric parameters, concrete volume, discharge capacity, and feasibility of the resulting designs. A solution was considered hydraulically and geometrically acceptable only if it satisfied all normalized constraints, including the head-ratio constraint, cycle-width ratio, apex-width ratio, magnification ratio, structural wall ratio, and design discharge requirement. This ensured that the final Pareto-optimal solutions were not only numerically optimal but also consistent with practical labyrinth spillway design limits.

Table 3 summarizes the comparison between the reference GA-based solution and the solutions obtained using the algorithms implemented in the present study.

Table 3. Verification comparison of optimized geometric parameters obtained from the reference GA-based study and the algorithms implemented in the present framework.

Design parameter	Symbol	Unit	Kardan et al. [10]	Reproduced GA	MOICA	MOPSO
Spillway width per cycle	w	m	23.655	21.019	17.220	21.600
Cycle length	B	m	33.976	32.143	28.950	32.150
Effective crest length per cycle	lc	m	73.591	72.203	67.100	71.851
Reference characteristic width	A_{ref}	m	10.001	9.311	6.820	8.100
Spillway height	P	m	7.896	7.111	5.460	7.010

Note: A_{ref} denotes the characteristic width reported in the reference GA-based study and is retained only for verification consistency. It should not be confused with the apex-width decision variable A used in the present optimization formulation and Table 1.

3.4 Performance Evaluation Metrics

Since multi-objective optimization produces a set of non-dominated solutions rather than a single optimum, algorithm performance was evaluated using metrics that quantify convergence, solution distribution, and objective-space coverage. In this study, three performance indicators were used: Spacing, Generational Distance, and Hypervolume.

The Spacing metric evaluates the uniformity of distribution of the obtained non-dominated solutions along the Pareto front. For each solution i, the minimum distance to the nearest neighboring solution was calculated as:

$$d_i = \min_{j \neq i} \sum_{k=1}^{M} \left| f_k^i - f_k^j \right| \quad (51)$$

where M is the number of objective functions, and f_k^i and f_k^j are the normalized values of the k[th] objective for solutions i and j, respectively. The Spacing metric was then calculated as:

$$S = \sqrt{\frac{1}{n-1} \sum_{i=1}^{n} (d_i - \bar{d})^2} \quad (52)$$

where n is the number of non-dominated solutions and $\bar{d}$ is the mean value of d_i. A smaller value of S indicates a more uniformly distributed Pareto front.

The Generational Distance metric measures the convergence of the obtained Pareto front toward a reference Pareto front. It was calculated as:

$$GD = \frac{\sqrt{\sum_{i=1}^{n} d_{i,ref}^2}}{n} \quad (53)$$

where $d_{i,ref}$ is the Euclidean distance between the i[th] obtained non-dominated solution and the nearest point on the reference Pareto front. In the absence of an analytically known true Pareto front, the reference front was constructed from the combined non-dominated solutions obtained from all independent runs and algorithms. A smaller value of GD indicates better convergence.

The Hypervolume indicator evaluates the objective-space coverage dominated by the obtained Pareto front with respect to a predefined reference point. It was calculated as:

$$HV = \lambda \left(\bigcup_{i=1}^{n} [f_i, r] \right) \quad (54)$$

where $\lambda(\cdot)$ denotes the Lebesgue measure, f_i is the objective vector of the i[th] non-dominated solution, and r is the reference point in the normalized objective space. A larger value of HV indicates better convergence and wider Pareto-front coverage.

For all performance metrics, the objective values were normalized before comparison to avoid bias caused by different physical units of discharge capacity and concrete volume. The metrics were calculated for each independent run, and the mean, best value, and standard deviation were used to assess both algorithmic performance and run-to-run robustness.

4 Results and Discussion

This section presents the optimization results obtained from the proposed scenario-based multi-objective framework. The results are analyzed in four stages. First, the algorithmic performance of MOPSO and MOICA is compared in terms of convergence behavior, Pareto-front distribution, Hypervolume, and robustness across independent runs. Second, the effects of design freedom are examined through the three optimization scenarios. Third, the representative boundary and compromise solutions are evaluated to clarify the trade-off between discharge capacity and concrete volume. Finally, the hydraulic and

engineering implications of the optimized geometries are discussed.

4.1 Algorithmic Performance and Pareto-Front Quality

The performance of MOPSO and MOICA was first evaluated using the same objective functions, constraints, parameter settings, population size, archive size, and stopping criterion. This ensured that the comparison reflected the intrinsic search behavior of the algorithms rather than differences in computational settings. Since both algorithms are stochastic, the comparison was based not only on the best solution obtained, but also on Pareto-front quality, convergence stability, Hypervolume, and run-to-run robustness.

4.1.1 Convergence behavior

The convergence histories of MOPSO and MOICA are shown in Figure 5. The curves indicate that MOPSO reached lower aggregated objective-function values more rapidly and with less oscillation than MOICA. During the early search stage, MOPSO exhibited a sharper reduction in the objective value, indicating faster movement toward promising regions of the feasible design space. In contrast, MOICA showed a slower and more fluctuating convergence pattern, which reflects its stronger exploratory behavior.

In the intermediate and final stages of the optimization process, MOPSO maintained a smoother convergence trajectory and approached stabilization earlier than MOICA. This behavior suggests a more effective balance between exploration and exploitation. MOICA, although capable of exploring broader regions of the search space, required more iterations to stabilize and showed greater variability in the convergence curve. Therefore, from a practical optimization perspective, MOPSO provided a more efficient and predictable convergence process for the labyrinth spillway design problem.

4.1.2 Pareto-front distribution and dominance

The Pareto fronts generated by MOPSO and MOICA are compared in Figure 6. Both algorithms produced feasible non-dominated solutions representing the trade-off between discharge capacity and concrete volume. However, the MOPSO objective-space solutions were consistently positioned in a more favorable region of the objective space, with higher discharge capacity for comparable concrete volumes and a smoother distribution of solutions along the front.

The improved distribution of MOPSO solutions indicates better coverage of the trade-off space and provides engineers with a more continuous range of design alternatives. This is particularly important in hydraulic-structure design, where the final selection is rarely based on a single optimum point. Instead, decision-makers often need to balance hydraulic safety, construction cost, geometric feasibility, and site-specific constraints. The more uniform and extended Pareto front obtained by MOPSO therefore provides more practical decision-support value than the more scattered MOICA front.

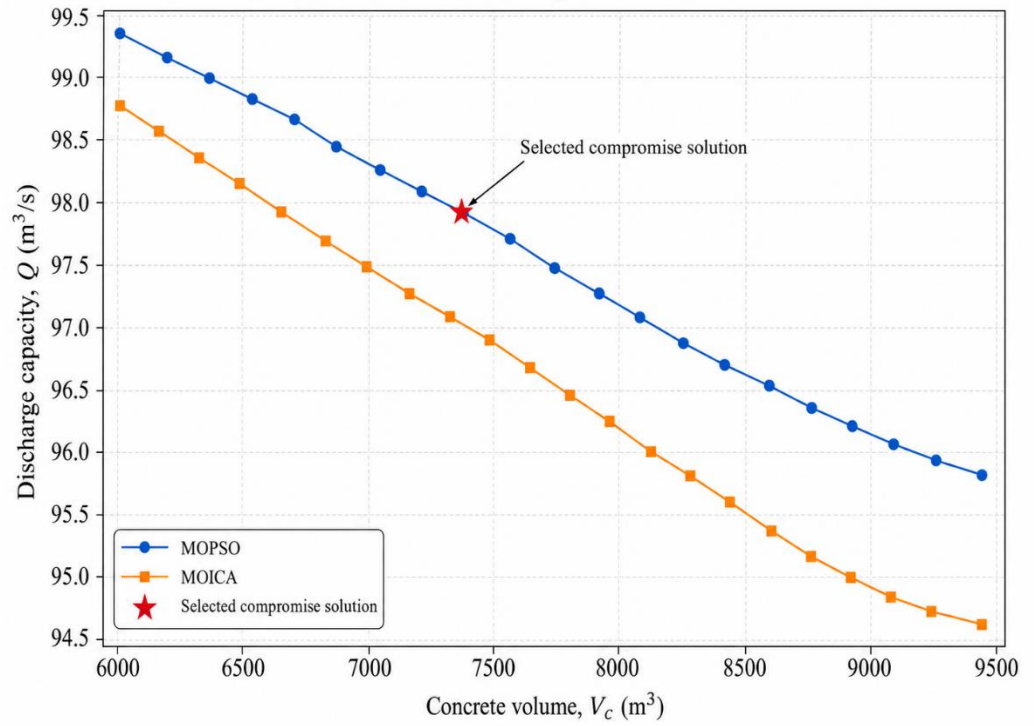


Figure 5. Comparison of objective-space solution trends obtained by MOPSO and MOICA. MOPSO provides higher discharge capacity than MOICA over comparable concrete-volume ranges, indicating a more favorable search performance and better hydraulic efficiency within the investigated solution space.

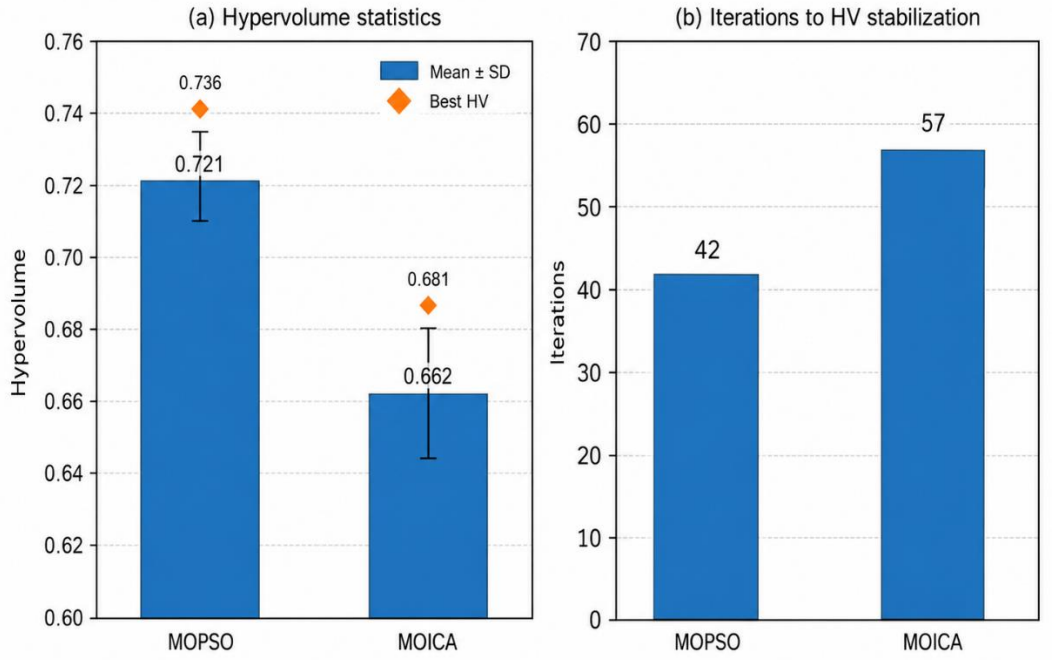


Figure 6. Hypervolume comparison and stability assessment of MOPSO and MOICA based on ten independent optimization runs: (a) mean Hypervolume values with standard deviation error bars and best Hypervolume markers; and (b) number of iterations required for Hypervolume stabilization. Higher Hypervolume values and earlier stabilization indicate better Pareto-front coverage and convergence stability.

Table 4. Hypervolume statistics obtained from ten independent optimization runs.

Indicator	MOPSO	MOICA
Best Hypervolume	0.736	0.681
Mean Hypervolume	0.721	0.662
Standard deviation	0.009	0.017
Iterations to Hypervolume stabilization	42	57

4.1.3 Hypervolume and robustness across independent runs

The Hypervolume statistics obtained from ten independent runs are summarized in Table 4. MOPSO achieved a higher mean Hypervolume value of 0.721 compared with 0.662 for MOICA, corresponding to an improvement of approximately 8.9%. The best Hypervolume value was also higher for MOPSO, with 0.736 compared with 0.681 for MOICA. In addition, the standard deviation of Hypervolume was lower for MOPSO, 0.009 compared with 0.017 for MOICA, indicating greater run-to-run stability.

MOPSO also reached Hypervolume stabilization after 42 iterations, whereas MOICA required 57 iterations. This confirms that MOPSO not only achieved better objective-space coverage but also reached a stable Pareto-front approximation earlier. The boxplot comparison of final objective values further supports this conclusion, showing narrower dispersion and fewer extreme variations for MOPSO. Overall, these results demonstrate that MOPSO provides a more robust and repeatable optimization performance, while MOICA remains useful as a complementary algorithm for exploratory search.

4.2 Scenario-Based Optimization Results

The scenario-based results were analyzed to evaluate how the level of geometric design freedom affects the hydraulic response of the optimized labyrinth spillway configurations. Figure 7 compares the volume–discharge response curves obtained for the three design scenarios. The results indicate that the imposed geometric and structural restrictions have a clear influence on the attainable discharge capacity. Scenario 1, which allowed the highest level of design freedom, provided the highest discharge capacity over the investigated concrete-volume range. Scenario 2 showed intermediate behavior, whereas Scenario 3, with the most restrictive design conditions, resulted in the lowest hydraulic performance.

The superior response of Scenario 1 can be attributed to the greater flexibility available for adjusting the geometric proportions of the labyrinth planform. When fewer variables are fixed, the optimization process can more effectively modify the sidewall angle, cycle length, apex width, spillway height, wall thickness, and number of cycles to obtain a more favorable balance between developed crest length and discharge coefficient. Conversely, when major dimensions are fixed, as in Scenarios 2 and 3, the feasible design space becomes narrower, and the algorithm has less freedom to compensate for hydraulic inefficiencies associated with unfavorable geometric proportions.

It is important to clarify that the response curves shown in Figure 7 should not be interpreted as conventional Pareto fronts in the strict multi-objective sense. The optimization problem in this study aims to minimize concrete volume and maximize discharge capacity. Therefore, any solution with both larger concrete volume and lower discharge capacity is dominated by a solution with smaller volume and higher discharge. Accordingly, the decreasing trends in Figure 7 should be interpreted as scenario-based hydraulic response curves, showing how geometric enlargement within the investigated solution range may reduce hydraulic efficiency when the resulting proportions become unfavorable.

This behavior is hydraulically meaningful for labyrinth spillways.

Increasing concrete volume may increase some structural dimensions or developed crest length, but the hydraulic benefit of this increase is not unlimited. If the resulting geometry intensifies nappe interference, local flow contraction, separation near apex regions, or partial submergence effects, the discharge coefficient may decrease and offset the advantage of increased crest length. Similar behavior has been reported in recent hydraulic and numerical studies of labyrinth-type spillway systems, where geometric configuration was shown to strongly affect flow structure, discharge coefficient, and overall hydraulic efficiency [25–27].

To quantify this response, representative low-volume and high-volume boundary solutions were extracted from each scenario. The low-volume boundary solution was used as the reference condition, and the high-volume boundary solution was compared with it to evaluate the corresponding percentage changes in concrete volume and discharge capacity. The percentage changes were calculated as:

$$\Delta V_c(\%) = \frac{V_{c,i} - V_{c,ref}}{V_{c,ref}} \times 100 \quad (55)$$

$$\Delta Q(\%) = \frac{Q_i - Q_{ref}}{Q_{ref}} \times 100 \quad (56)$$

where $V_{c,i}$ and Q_i are the concrete volume and discharge capacity of a given Pareto solution, while $V_{c,ref}$ and Q_{ref} are the corresponding values for the low-volume boundary solution in the same scenario.

As shown in Table 5, increasing the concrete volume from 6000 m^3 to 9500 m^3 resulted in a 58.33% increase in structural volume for all three scenarios. However, the discharge capacity decreased by 3.52%, 4.36%, and 4.41% in Scenarios 1, 2, and 3, respectively. This confirms that the high-volume boundary solutions should not be regarded as maximum-discharge solutions. Rather, they represent geometrically larger configurations located at the high-volume end of the investigated response range.

Figure 8 further illustrates the percentage changes in concrete volume and discharge capacity between the low-volume and high-volume boundary solutions. Although the increase in concrete volume was identical in all scenarios, the reduction in discharge capacity became slightly more pronounced as the design constraints became more restrictive. Scenario 1 showed the smallest discharge reduction, indicating that greater geometric freedom helped reduce the hydraulic penalty associated with increasing structural dimensions. In contrast, Scenario 3 showed the largest reduction, suggesting that restrictive geometric conditions made the system more sensitive to unfavorable proportional changes.

Table 5. Representative boundary solutions obtained from the scenario-based volume–discharge response curves.

Scenario	Design point	Concrete volume, V_c (m^3)	Discharge capacity, Q (m^3/s)	$\Delta V_c(\%)$	$\Delta Q(\%)$
Scenario 1	Low-volume boundary solution	6000	99.40	—	—
Scenario 1	High-volume boundary solution	9500	95.90	+58.33	-3.52
Scenario 2	Low-volume boundary solution	6000	98.70	—	—
Scenario 2	High-volume boundary solution	9500	94.40	+58.33	-4.36
Scenario 3	Low-volume boundary solution	6000	97.60	—	—
Scenario 3	High-volume boundary solution	9500	93.30	+58.33	-4.41

From an engineering perspective, these results highlight an important design principle: larger labyrinth spillway geometries do not automatically provide better hydraulic performance. The discharge capacity is governed not only by the developed crest length but also by the efficiency of the geometric configuration. Therefore, practical design should focus on balanced geometric proportions rather than structural enlargement alone. Scenario 1 provides the most favorable response because it offers greater flexibility for maintaining efficient proportions. Scenario 2 may represent a more realistic rehabilitation condition where some major dimensions are fixed, while Scenario 3 illustrates the performance limitations that can arise when design freedom is strongly restricted.

Overall, the scenario-based analysis demonstrates the value of incorporating different levels of design freedom into the optimization framework. It allows the designer to distinguish between geometrically larger but hydraulically less efficient configurations and more balanced solutions that better satisfy both hydraulic and structural requirements.

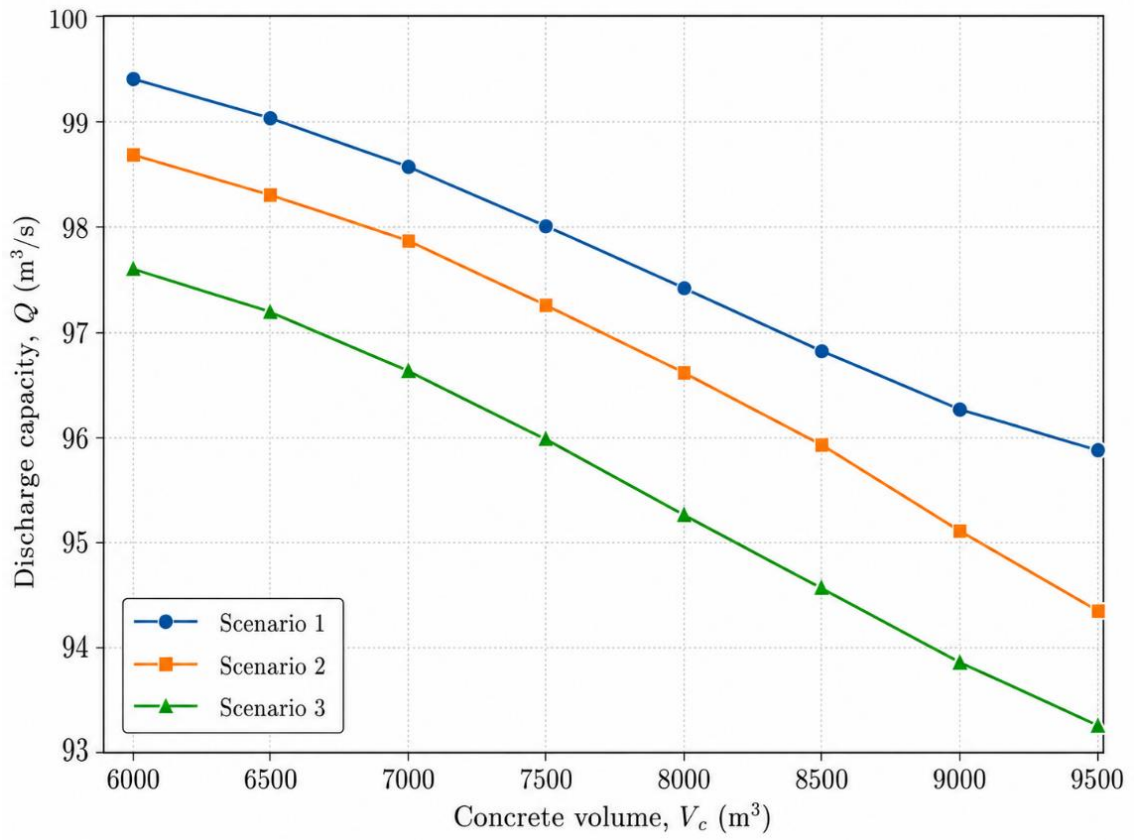


Figure 7. Scenario-based volume–discharge response curves obtained under different levels of geometric design freedom. Scenario 1 provides the highest discharge capacity over the investigated concrete-volume range.

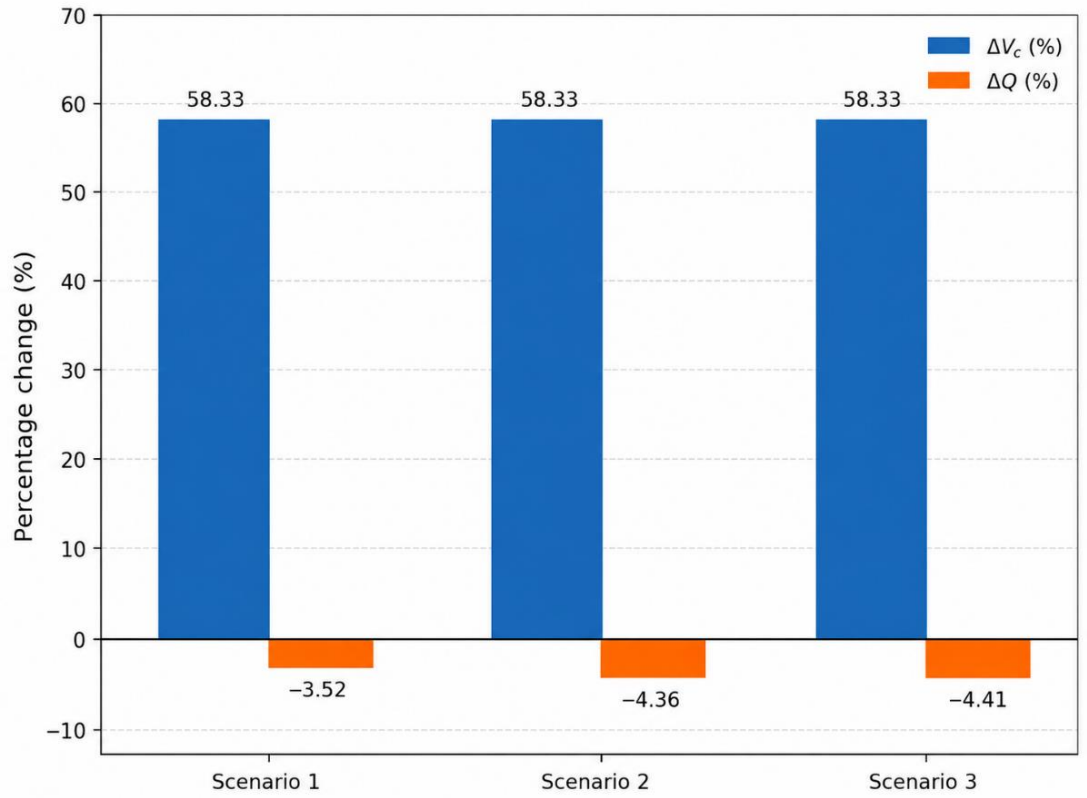


Figure 8. Percentage changes in concrete volume and discharge capacity between the low-volume and high-volume boundary solutions for each scenario. The results show that increasing concrete volume by 58.33% reduced discharge capacity by 3.52–4.41%, indicating that hydraulic efficiency depends on optimized geometric proportions rather than structural enlargement alone.

As shown in Figure 8, all scenarios experienced the same concrete-volume increase of 58.33%, but the reduction in discharge capacity became slightly more pronounced as the design constraints became more restrictive. Scenario 1 showed the smallest discharge reduction -3.52%, whereas Scenarios 2 and 3 showed larger reductions of -4.36% and -4.41%, respectively. This indicates that additional geometric freedom allows the optimization process to better compensate for hydraulic inefficiencies. Conversely, when major dimensions are fixed, larger configurations are more likely to deviate from hydraulically favorable proportions, leading to reduced discharge efficiency.

4.3 Hydraulic Interpretation of the Non-Monotonic Volume–Discharge Response

The decreasing volume–discharge response observed in Section 4.2 requires further hydraulic interpretation because it may appear counter-intuitive if concrete volume is assumed to be directly proportional to hydraulic performance. In labyrinth spillways, however, discharge capacity is not governed by structural size alone. According to the governing discharge equation, the discharge capacity depends on both the developed crest length and the discharge coefficient:

$$Q = \frac{2}{3} C_d L_c \sqrt{2g} H_T^{\frac{3}{2}} \quad (57)$$

where C_d is the discharge coefficient and L_c is the total developed crest length. Therefore, an increase in geometric

dimensions or concrete volume can improve discharge capacity only if the corresponding geometric changes do not reduce the hydraulic efficiency of the spillway. If the enlarged configuration produces unfavorable flow conditions, such as nappe interference, local flow contraction, partial submergence, or flow separation near the apex regions, the resulting decrease in C_d may offset or even exceed the benefit of increasing L_c. This explains why larger structural configurations do not necessarily produce higher discharge capacity.

To evaluate the material efficiency of the investigated configurations, a volume-normalized hydraulic productivity index was defined as:

$$E_Q = \frac{Q}{V_c} \tag{58}$$

where E_Q represents the discharge capacity provided per unit concrete volume. A higher value of E_Q indicates a more material-efficient hydraulic design. To compare the low-volume and high-volume boundary solutions within each scenario, the normalized productivity index was calculated as:

$$E_Q^* = \frac{E_{Q,i}}{E_{Q,ref}} = \frac{Q_i/Q_{ref}}{V_{c,i}/V_{c,ref}} \tag{59}$$

where $E_{Q,i}$ is the productivity index of a given boundary solution, and $E_{Q,ref}$ is the productivity index of the low-volume reference solution in the same scenario. The percentage change in hydraulic productivity was then calculated as:

$$\Delta E_Q(\%) = (E_Q^* - 1) \times 100 \tag{60}$$

Table 6 summarizes the volume-normalized hydraulic productivity of the low-volume and high-volume boundary solutions.

As shown in Table 6, the high-volume boundary solutions exhibit substantially lower hydraulic productivity than the corresponding low-volume boundary solutions. Although the concrete volume increased by 58.33%, the discharge capacity decreased slightly, which caused the volume-normalized productivity to decline by approximately 39.07%, 39.59%, and 39.62% in Scenarios 1, 2, and 3, respectively. This finding confirms that the high-volume configurations are not hydraulically or materially efficient, even though they contain larger structural dimensions.

The productivity analysis provides a clearer explanation of the non-monotonic response observed in Figure 7 and Figure 8. The reduction in E_Q indicates that additional concrete volume did not translate into proportional hydraulic benefit. Instead, the enlarged configurations likely moved away from hydraulically favorable proportions, reducing the effective discharge contribution of the developed crest length. This interpretation is consistent with the known hydraulic behavior of labyrinth spillways, where performance depends strongly on geometric proportion, nappe behavior, effective crest contribution, and discharge-coefficient variation.

Table 6. Volume-normalized hydraulic productivity of the low-volume and high-volume boundary solutions.

Scenario	Design point	V_c (m³)	Q (m³/s)	$E_Q = Q/V_c$	E_Q^*	$\Delta E_Q(\%)$
Scenario 1	Low-volume boundary solution	6000	99.40	0.01657	1.000	—
Scenario 1	High-volume boundary solution	9500	95.90	0.01009	0.609	-39.07
Scenario 2	Low-volume boundary solution	6000	98.70	0.01645	1.000	—
Scenario 2	High-volume boundary solution	9500	94.40	0.00994	0.604	-39.59
Scenario 3	Low-volume boundary solution	6000	97.60	0.01627	1.000	—
Scenario 3	High-volume boundary solution	9500	93.30	0.00982	0.604	-39.62

From a design perspective, the results show that the most efficient configurations are not necessarily the largest ones. The low-volume boundary solutions provided both higher discharge capacity and higher hydraulic productivity within the investigated response range. Therefore, the optimization process should focus on identifying balanced geometric configurations rather than simply increasing structural dimensions. This is particularly important in spillway rehabilitation projects, where unnecessary increases in concrete volume may increase construction cost without improving hydraulic capacity. The proposed scenario-based framework is useful because it identifies when geometric enlargement becomes hydraulically inefficient and helps guide the selection of designs that better balance hydraulic performance and material use.

4.4 Engineering Implications and Design Recommendations

The optimization results provide several practical implications for labyrinth spillway design and rehabilitation. The most important finding is that hydraulic efficiency is governed by balanced geometric proportions rather than by structural enlargement alone. Although increasing concrete volume may increase some geometric dimensions, it does not necessarily improve discharge capacity if the resulting configuration reduces the effective discharge coefficient. Therefore, design decisions should not be based solely on increasing crest length, spillway height, or wall dimensions, but should consider the combined effects of developed crest length, sidewall angle, apex width, cycle width, and head ratio.

From a practical design perspective, Scenario 1 produced the most favorable hydraulic response because it allowed greater flexibility in adjusting the main geometric variables. This suggests that when the design conditions permit sufficient geometric freedom, multi-objective optimization can identify configurations with better hydraulic performance and material efficiency. However, such flexibility may not always be available in rehabilitation projects, where existing dam geometry, available channel width, structural constraints, and construction limitations may restrict the feasible design space.

Scenario 2 represents a more realistic rehabilitation condition because major dimensions such as spillway height and available width are often fixed by the existing site. Although its hydraulic response was less favorable than Scenario 1, it still provided a useful range of design alternatives. This indicates that even under partially constrained conditions, multi-objective optimization can help identify efficient configurations and avoid unnecessary structural enlargement.

Scenario 3 showed the most restricted hydraulic performance because several key geometric and structural parameters were fixed. The results from this scenario demonstrate that when design freedom is strongly limited, the optimization algorithm has less ability to compensate for unfavorable geometric proportions. This may lead to lower discharge capacity and reduced hydraulic productivity. Therefore, highly constrained designs should be evaluated carefully before implementation, especially when the objective is to improve spillway capacity without excessive construction cost.

The results also highlight the importance of avoiding misleading design interpretations. The high-volume boundary solutions in this study should not be considered optimal merely because they contain more concrete or larger dimensions. In fact, these configurations showed lower discharge capacity and lower volume-normalized hydraulic productivity than the corresponding low-volume boundary solutions. This finding supports the use of objective-space analysis, productivity indices, and scenario-based evaluation before selecting a final design.

For engineering decision-making, the selected design should be located in a balanced region of the solution space where discharge capacity, concrete volume, constructability, and hydraulic feasibility are simultaneously acceptable. Extreme solutions may be useful for understanding the limits of the design space, but they are not always suitable for implementation. A low-volume solution may be attractive from an economic perspective, while a high-capacity solution may be preferred for safety considerations. However, the final compromise solution should avoid configurations that increase concrete volume without improving hydraulic performance.

5 Conclusions

This study developed a scenario-based multi-objective optimization framework for the geometric design of labyrinth spillways by coupling empirical hydraulic relationships with MOPSO and MOICA. The optimization problem was formulated to maximize discharge capacity and minimize concrete volume under hydraulic, geometric, structural, and design-discharge constraints. The Ute Dam labyrinth spillway was used as a real-world benchmark case. The algorithmic comparison showed that MOPSO outperformed MOICA in terms of Pareto-front quality, convergence stability, and robustness. Across ten independent runs, MOPSO achieved a higher mean Hypervolume value of 0.721 compared with 0.662 for MOICA, a higher best Hypervolume value of 0.736 compared with 0.681, and a lower standard deviation of 0.009 compared with 0.017. MOPSO also reached Hypervolume stabilization earlier, after 42 iterations compared with 57 iterations for MOICA. These results indicate that MOPSO provides more stable and better-distributed solutions for the present constrained spillway optimization problem. The scenario-based analysis showed that geometric design freedom strongly affects hydraulic response. Scenario 1, with the highest design flexibility, produced the most favorable volume–discharge response, while Scenario 3, with the most restrictive conditions, showed the lowest hydraulic performance. A key finding was that increasing concrete volume alone did not improve discharge capacity. Increasing the volume from 6000 m^3 to 9500 m^3 increased structural volume by 58.33%, but reduced discharge capacity by 3.52–4.41%. The volume-normalized hydraulic productivity also decreased by approximately 39%, confirming that hydraulic efficiency depends on balanced geometric proportions rather than structural enlargement alone. The proposed framework provides a practical decision-support tool for labyrinth spillway design and rehabilitation. It enables engineers to compare alternative design scenarios, evaluate algorithmic robustness, and identify efficient configurations that balance hydraulic performance and concrete volume. MOPSO is recommended as the primary optimizer for this class of constrained multi-objective design problems, while MOICA can be used as a complementary exploratory benchmark. Future studies may extend the framework by incorporating CFD-based discharge-coefficient evaluation, uncertainty analysis, structural safety, sediment and scour constraints, and life-cycle cost assessment.

Funding statement: This research received no external funding.

Conflict of Interest: The authors declare that they have no conflict of interest.

AI Statement: The authors acknowledge the use of artificial intelligence (AI) tools to assist with English language editing, grammar improvement, enhancement of clarity and readability, and preparation of preliminary schematic flowcharts. All scientific content, mathematical formulation, technical interpretations, optimization results, figures, and final revisions were checked, verified, and approved by the authors.

References

1. Chow VT. Open-channel hydraulics. New York: McGraw-Hill; 1959.
2. U.S. Bureau of Reclamation. Design of small dams. 3rd ed. Washington (DC): U.S. Government Printing Office; 1987.
3. Novak P, Guinot V, Jeffrey A. Hydraulic modelling: an introduction. London: Spon Press; 2007.
4. Tullis BP, Amanian N, Waldron D. Head-discharge relationships for labyrinth weirs. Journal of Hydraulic Engineering. 1995;121(3):247–255.
5. Crookston BM, Tullis BP. Hydraulic design and analysis of labyrinth weirs. I: Discharge relationships. Journal of Irrigation and Drainage Engineering. 2013;139(5):363–370.
6. Lux FH, Hinchliff DL. Design and construction of labyrinth spillways. In: Proceedings of the 15th International Congress on Large Dams; 1985. p. 1–15.
7. Erpicum S, Archambeau P, Dewals B, Pirotton M. Three-dimensional numerical modeling of free-surface flow over piano key and labyrinth spillways. Journal of Hydraulic Research. 2016;54(4):412–426.
8. Azimi AH, Zarrati AR. Numerical investigation of labyrinth spillway performance under varying head conditions. Journal of Hydraulic Engineering. 2023;149(3):04022095.
9. Pasquier R, Erpicum S, Archambeau P, Dewals B, Pirotton M. Design guidelines for piano key and labyrinth spillways: A comprehensive review. Water. 2024;16(2):321–345.
10. Kardan N, Hassanzadeh Y, Shakooei Bonab B. Shape optimization of trapezoidal labyrinth weirs using genetic algorithm. Arabian Journal for Science and Engineering. 2017; 42:1219–1229.
11. Hosseini K, Nodoushan EJ, Barati R, Shahheydari H. Optimal design of labyrinth spillways using meta-heuristic algorithms. KSCE Journal of Civil Engineering. 2016;20(1):468–477.
12. Ferdowsi A, Farzin S, Mousavi SF, Karami H. Hybrid Bat & Particle Swarm Algorithm for optimization of labyrinth spillway based on half & quarter round crest shapes. Flow Measurement and Instrumentation. 2019; 66:209–217.
13. Jafari-Asl J, Ben Seghier MEA, Ohadi S, van Gelder P. Efficient method using Whale Optimization Algorithm for reliability-based design optimization of labyrinth spillway. Applied Soft Computing. 2021; 101:107036.
14. Mahmoud A, Yuan X, Hajilounezhad T, Yuan Y. Investigation on labyrinth spillway multi-objective optimization with an emphasis on predicting discharge coefficient through different artificial neural networks. Measurement. 2021; 174:109036.
15. Campisano A, Modica C, Siciliano C, Ventura G. Optimization of labyrinth spillway geometry for enhanced discharge capacity. Water Resources Management. 2021;35(7):2345–2362.
16. Falvey HT. Cavitation in chutes and spillways. Denver (CO): U.S. Bureau of Reclamation; 2003.
17. Ferdowsi A, Valikhan-Anaraki M, Mousavi SF, Farzin S, Mirjalali S. Developing a model for multi-objective optimization of open channels and labyrinth weirs: Theory and application in Isfahan irrigation networks. Flow Measurement and Instrumentation. 2021; 80:108–124.
18. Kennedy J, Eberhart R. Particle Swarm Optimization. In: Proceedings of IEEE International Conference on Neural Networks; 1995.
19. Atashpaz-Gargari E, Lucas C. Imperialist Competitive Algorithm: An algorithm for optimization inspired by imperialistic competition. In: IEEE Congress on Evolutionary Computation; 2007.
20. Deb K, Pratap A, Agarwal S, Meyarivan T. A fast and elitist multiobjective genetic algorithm: NSGA-II. IEEE Transactions on Evolutionary Computation. 2002;6(2):182–197.
21. Zitzler E, Brockhoff D, Thiele L. The hypervolume indicator revisited. In: Proceedings of the 2003 Congress on Evolutionary Computation; 2003.
22. Premkumar M, Jangir P, Sowmya R, et al. MOSMA: Multi-objective slime mould algorithm. IEEE Access. 2021; 9:3229–3248.
23. Bozorg Haddad O, Mirmomeni M, Mariño MA. Optimal design of stepped spillways using the HBMO algorithm. Civil Engineering and Environmental Systems. 2010;27(1):81–94.
24. Tullis BP, Young JC, Chandler MA. Head-discharge relationships for submerged labyrinth weirs. Journal of Hydraulic Engineering. 2007;133(3):248–254.
25. Crookston BM, Erpicum S, Tullis BP,

Laugier F. Hydraulics of labyrinth and piano key weirs: 100 years of prototype structures, advancements, and future research needs. Journal of Hydraulic Engineering. 2019;145(12):03119002.
26. Aydin MC, Ulu AE. Numerical investigation of labyrinth-shaft spillway. Applied Water Science. 2023; 13:89.
27. Shehata AH, Samy M, Ibrahim MM, et al. Optimizing trapezoidal labyrinth weir design for enhanced scour mitigation in straight channels. Water. 2024;16(17):2443.
28. Asgharzadeh-Bonab A, Bijanvand S, Parsaie A, Afaridegan E. Machine learning-based estimation of discharge coefficient for semicircular labyrinth weirs. Scientific Reports. 2025; 15:33002.



© 2026 by the authors. Licensee SCU, Ahvaz, Iran. This article is an open access article distributed under the terms and conditions of the Creative Commons Attribution 4.0 International (CC BY 4.0 license) (http://creativecommons.org/licenses/by/4.0/).